

ISABELLE Project

Technical Note No. 332

DIPOLE MAGNET END DESIGN

Richard C. Fernow

December 1981

We examine the assumptions used in the 2-D end design. A comparison with the measurements from LM1 show that the model can qualitatively reproduce the main features in the data. We then calculate a modification to the LM3 end spacers which should improve the integrated sextupole and decapole fields from the ends.

Introduction

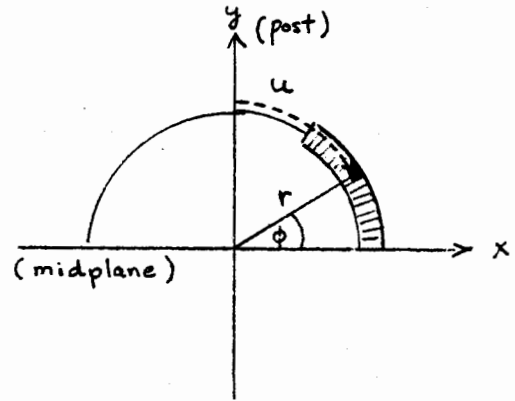
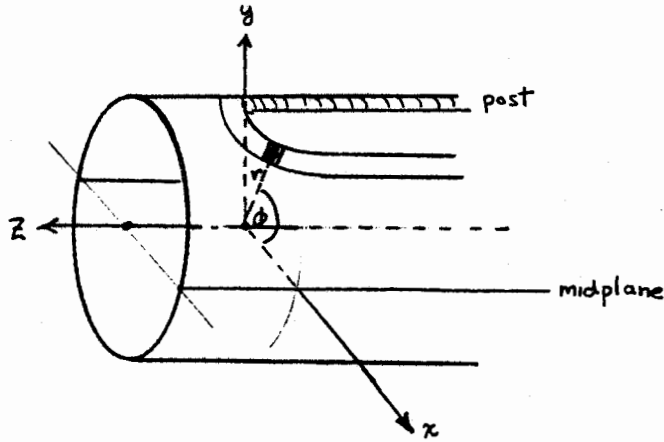
By its nature a proper treatment of the fields in the end of the magnet must be three dimensional. This is not convenient in a design program using minimization techniques however since hundreds or thousands of iterations are involved in the minimization. In a three dimensional calculation each minimization iteration would also involve loops over hundreds of current elements. A proper calculation must also take into account the nearby presence of iron in the straight section.

In addition to the theoretical problems it is experimentally very difficult to make the cables conform to the required shape in the curved section of the end. The average thickness per turn typically increases by several mils as the cable moves from the straight section to the post region of the curve. Finally there are problems with the cable crossing thru some spacers and asymmetries resulting from the leads leaving the magnet.

For these reasons the original design of the dipole ends (R. Palmer, TLM-10, 22) made use of a two-dimensional, iron-free approximation. The philosophy taken was that the two dimensional calculations would give a sufficiently accurate description of the ends so that the calculations could be compared with measurements and then the end parameters could be re-adjusted empirically. In section 2 of this report we outline the two dimensional theory and show that despite its limitations it does indeed reproduce the main features of the data. Then in section 3 we describe the first iteration on the end design which will hopefully make the ends more self-correcting.

2-D Theory of the End Spacers

Consider a small block of conductor in the dipole. In the straight section of the magnet the conductor block will have a constant r and ϕ in a cylindrical coordinate system. In the end region the coil block moves toward the post as Z

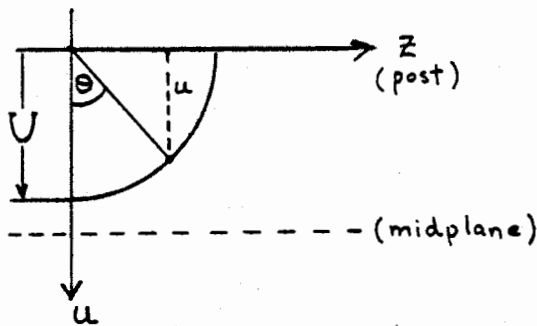


increases. The end design chosen by R. Palmer requires that the ^{unfolding} ~~projection~~ of the end portion of the conductor onto the x-z plane (midplane) should be a circle. It is convenient to express this requirement in terms of the arc length u from the post to a point (r, ϕ) in the conductor block. These are related by:

$$u = r\left(\frac{\pi}{2} - \phi\right) \tag{1}$$

Then, if we make a plot of u versus Z as the conductor moves thru the end region, the midplane circle requirement mentioned above is equivalent to the requirement that $u(Z)$ is a circle as well:

$$u(Z) = \sqrt{U^2 - Z^2} \tag{2}$$



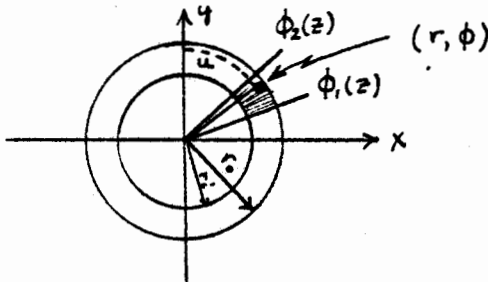
where U is the arclength in the straight section.

Since the current elements always lie on a cylindrical surface the current density J will only have \hat{z} and $\hat{\phi}$ components. The position vector R from the current element to the observation point on the other hand will only have \hat{z} and \hat{r} components. The elemental field contributions at the observation point have directions $d\mathbf{B} = d\mathbf{j} \times \hat{R}$. This leads to three classes of contributions to the field at the point $Z=Z_0$.

- (I) $\hat{J}_Z \times \hat{R}_R$
- (II) $\hat{J}_\phi \times \hat{R}_Z$
- (III) $J_\phi \times \hat{R}_R$

If we consider points on the magnet axis the sum of the Class III contributions over the four quadrants vanishes for any Z . Every current element in the magnet with $J_Z \neq 0$ will give a Class I contribution in the same direction to the field at Z . However the current element at $Z = Z_0$ will generally give the largest contribution because of the $\sin\theta/R^2$ dependence of the field. Class II contributions only arise from the curved part of the ends. Curved elements to the left and right of Z_0 will give contributions of opposite directions to the field at Z_0 . In the two dimensional approximation we neglect Class II contribution and only consider Class I contributions from current elements at Z_0 .

Now consider a cross section of a coil block at a fixed Z in the end section. We define $Z = 0$ here to be the end of the straight section. The contribution of



the current elements at Z to the multipole field is:

$$B_n(Z) = \frac{\mu_0}{2\pi} \int_{r_1}^{r_0} \int_{\phi_1(Z)}^{\phi_2(Z)} j_Z(Z) \frac{\cos(n+1)\phi}{r^{n+1}} r d\phi dr \quad (3)$$

Note that the limits of the ϕ integration depend on Z . As we move further away from the end of the straight section the curved block moves closer to the post. It follows from Eqs. (1) and (2) that for elements on the cylindrical surface at r

$$\phi_1(Z) = \frac{\pi}{2} - \frac{\sqrt{U_1^2 - Z^2}}{r} \quad (4)$$

where U_1 is the arc length of the block edges in the straight section we see from the arclength versus Z plot that

$$j_z(Z) = j_0 \cos\theta = \frac{\bar{r}I}{\bar{t}(r_0 - r_1)} \frac{1}{r} \frac{r(\frac{\pi}{2} - \phi)}{\sqrt{r^2(\frac{\pi}{2} - \phi)^2 + z^2}} \quad (5)$$

If we substitute (5) back into (3) we get

$$B_n(Z) = \frac{\mu_0}{2\pi} \frac{\bar{r}I}{\bar{t}(r_0 - r_1)} \int_{r_1}^{r_0} \int_{\phi_1(Z)}^{\phi_2(Z)} \frac{\cos(n+1)\phi}{r^n} \frac{(\frac{\pi}{2} - \phi)}{\sqrt{r^2(\frac{\pi}{2} - \phi)^2 + z^2}} d\phi dr \quad (6)$$

We will use equation (6) to find the contribution to any multipole of the curved parts of the ends at any Z although this is not the form that the minimization program uses. Table I defines the 7 end blocks used in the TLM-22 design. The quantity \bar{d} is the length of straight section from the end of the iron to the start of the curved section at the radius r , while \bar{U}_1 and \bar{U}_2 are the radii of the circles projected on the midplane by current elements from the edges of the block and at radius r .

Figures 1, 2, and 3 give the Z dependence of the dipole, sextupole, and decapole predicted by Eq. (6). Also plotted are end measurements of LM1 (provided by H. Kirk). We see that, even though the calculations and measurements do not agree quantitatively, they exhibit the same qualitative trends and thus the iterative philosophy outlined in Section 1 makes sense. In particular it is gratifying that the model gives the large B_2 and B_4 peaks and zeroes in the right places.

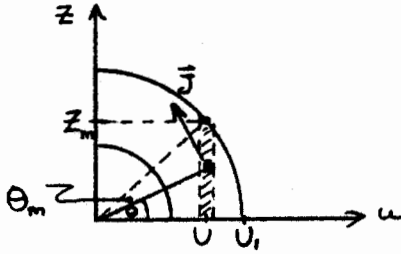
In the end design we are actually interested in the end field integrated along the Z axis. For this purpose it is most convenient to consider a fixed current block at the end of the straight section and then to use an average j_z appropriate to each (r, ϕ) element. Thus we write:

$$\int B_n dZ = \frac{\mu_0}{2\pi} \int_{r_1}^{r_0} \int_{\phi_1}^{\phi_2} \bar{j}_z(r, \phi) \frac{\cos(n+1)\phi}{r^{n+1}} r dr d\phi \quad (7)$$

where using Eq. (5)

$$\bar{J}_z(r, \phi) = j_0 \int_0^{z_m} \cos \theta(z) dz \quad (8)$$

It is useful to consider the meaning of this integral using a Z-u plot. By



Eq. (1) the fixed (r, ϕ) point corresponds to a fixed value of $u = U$. Using

$$\tan \theta = \frac{z}{U} \quad (9)$$

we can rewrite (8) in terms of $d\theta$ as

$$\begin{aligned} \bar{J}_z &= j_0 U \int_0^{\theta_m} \sec \theta d\theta \\ &= j_0 U \ln (\sec \theta_m + \tan \theta_m) \end{aligned} \quad (10)$$

Finally if we make the substitution

$$a = \cos \theta_m = \frac{U}{U_1} \quad (11)$$

we can express the integral in a form originally derived by R. Palmer,

$$\bar{J}_z(r, \phi) = j_0 r \left(\frac{\pi}{2} - \phi \right) \ln \left[\frac{1 + \sqrt{1 - a^2}}{a} \right] \quad (12)$$

We have found numerically that the r dependence in Eq. (12) is sufficiently weak so that one may simply evaluate the function at r . The final result then is that Eq. (7) can be written

$$\int B_n dZ = \frac{\mu_0}{2\pi} R(r) \int_{\phi_1}^{\phi_2} \bar{J}_2(\bar{r}, \phi) \cos(n+1)\phi d\phi \quad (13)$$

where $R(r)$ is a closed analytic expression resulting from the r integration.

In Table II we list the contributions of each of the 7 end coil blocks to B_0 , B_2 , and B_4 . The straight part column gives the field per unit length while the curved part column is the total integrated field. It is possible to make the ends self-correcting by adjusting the lengths of the end straight parts in such a way that the sum of integrated straight and curved parts is zero for B_2 , B_4 , etc. Note that as soon as the conductors leave the iron the straight section field no longer has $B_4 = 0$, etc.

The first column of Table III shows the sum of the curved part integrated multipoles. Note that B_2 thru B_8 are all negative. In order to cancel this the straight part of the end must contribute a corresponding positive integrated field. For B_2 and B_4 together this can only be done with blocks 1 and 5, and we see in Table I that these blocks have the largest values of \bar{d} .

New End Design

We list the integrated straight end field for the TLM-22 design in Table III. The next column lists the total design fields. This column is not 0 for B_2 and higher moments because of two minor errors in the original design program. The next column gives measurements for LM1 integrated from $Z = 87$ to 102 inches (provided by H. Kirk). We see that the measured values are larger than the calculated ones. Part of this effect comes from the fact that the average conductor thickness grows by several mils as it leaves the straight section and rounds the post. We estimate that this is responsible for an increase of approximately 1.1 B_2 units and 0.4 B_4 units in Table III.

The column headed Δ gives the total deviation of the LM1 measurements from the original design values. The new design should aim at the negative of these values so that the actual magnet will have 0 end fields. The issue is complicated however by the fact that new magnets will use a thinner conductor ($t = 55.0$ mils) and will have 4 additional turns per quadrant. Thus we will probably need a third iteration. The calculated multipoles using the $t = 55$ mil cross section and d values from TLM-22 is shown on Table III. It can be seen that this change alone probably would have improved the integrated B_2 and degraded B_4 .

For expediency this design iteration was restricted to only vary the quantities d_1 and d_5 together by the same amount. The result was to shorten d_1 and d_5 by 0.17 cm, giving the integrated multipoles in the last column of Table III. The end spacers for LM3 have been shortened accordingly. For references we give a summary of this new intermediate design in Table IV.

TABLE I
TLM-22 End Design

Block	N	ϕ_{start}	ϕ_{end}	r_i (cm)	r_o (cm)	\bar{d} (cm)	\bar{U}_1 (cm)	\bar{U}_2 (cm)
1	20	0.040 ^o	24.055	6.566	7.348	10.37	8.01	10.92
2	20	24.055	48.071	6.566	7.348	5.89	5.09	8.01
3	19	48.071	70.885	6.566	7.348	3.25	2.32	5.09
4	4	75.785	80.588	6.566	7.348	2.00	1.14	1.73
5	10	0.040	10.764	7.399	8.181	9.07	10.77	12.23
6	17	10.764	28.994	7.399	8.181	2.00	8.29	10.77
7	11	33.959	45.755	7.399	8.181	2.00	6.02	7.62

TABLE II

End Block Contributions to End Multipoles

Block		straight part $\left(\frac{G}{A\text{-cm}^n}\right)$	curved part $\left(\frac{G}{A\text{-cm}^n} \times \text{cm}\right)$
B_0	1	2.241	18.30
	2	1.852	10.05
	3	1.106	3.40
	4	0.094	0.11
	5	1.024	10.31
	6	1.641	13.22
	7	0.869	4.83
$10^2 \times B_2$	1	3.622	6.84
	2	-1.400	-18.27
	3	-4.287	-14.62
	4	-0.555	- 0.64
	5	1.616	6.44
	6	1.410	- 2.56
	7	-0.911	- 9.13
$10^4 \times B_4$	1	4.105	- 6.84
	2	-8.268	-24.70
	3	3.684	20.65
	4	1.703	2.03
	5	2.432	5.22
	6	-0.706	-16.01
	7	-2.812	- 6.32

TABLE III

Integral Multipoles for Dipole End $\left[\frac{G}{A\text{-cm}^n} \times \text{cm} \right]$

	TLM-22 Curved	TLM-22 Straight	TLM-22 Total	LMI Measurement	Δ	$\bar{t} = 55$ Calculation	This Design	
B_0	60	52	112	137	----	117	116	
$10^2 \times B_2$	-31.93	29.94	- 1.99	1.22	3.21	- 2.42	- 3.35	-.9
$10^4 \times B_4$	-25.99	24.26	- 1.73	5.80	7.53	- 0.46	- 1.62	-.0
$10^6 \times B_6$	-30.70	29.56	- 1.14	----	----	- 2.85	- 3.70	-.04
$10^8 \times B_8$	-42.20	14.81	-27.39	----	----	-30.07	-29.46	-.0

TABLE IV
New Dipole End Design

Block	N	ϕ_{start}	ϕ_{end}	$\Delta\phi$	\bar{r}_1 (cm)	\bar{r}_o (cm)	\bar{d} (cm)	\bar{U}_1 (cm)	\bar{U}_2 (cm)
1	21	0.040 ^o	24.201	24.16	6.566	7.348	10.20	7.99	10.92
2	21	24.201	48.362	24.16	6.566	7.348	5.89	5.05	7.99
3	20	48.362	71.373	23.01	6.566	7.348	3.25	2.26	5.05
4	4	75.988	80.590	4.60	6.566	7.348	2.00	1.14	1.70
5	10	0.040	10.315	10.28	7.399	8.181	8.90	10.83	12.23
6	18	10.315	28.810	18.49	7.399	8.181	2.00	8.32	10.83
7	11	34.458	45.760	11.30	7.399	8.181	2.00	6.01	7.55

Figure 1

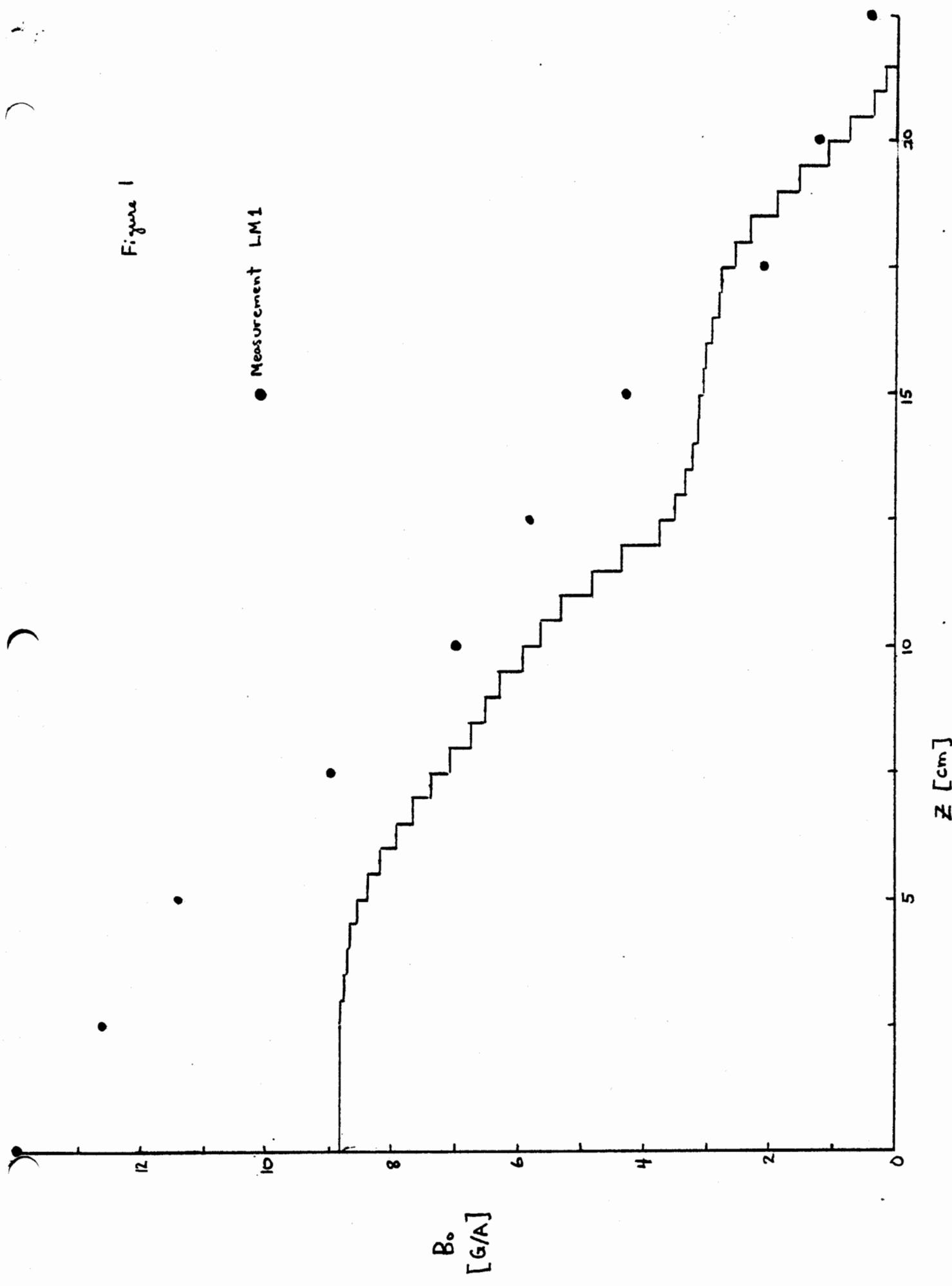


Figure 2

● Measurement LM-1

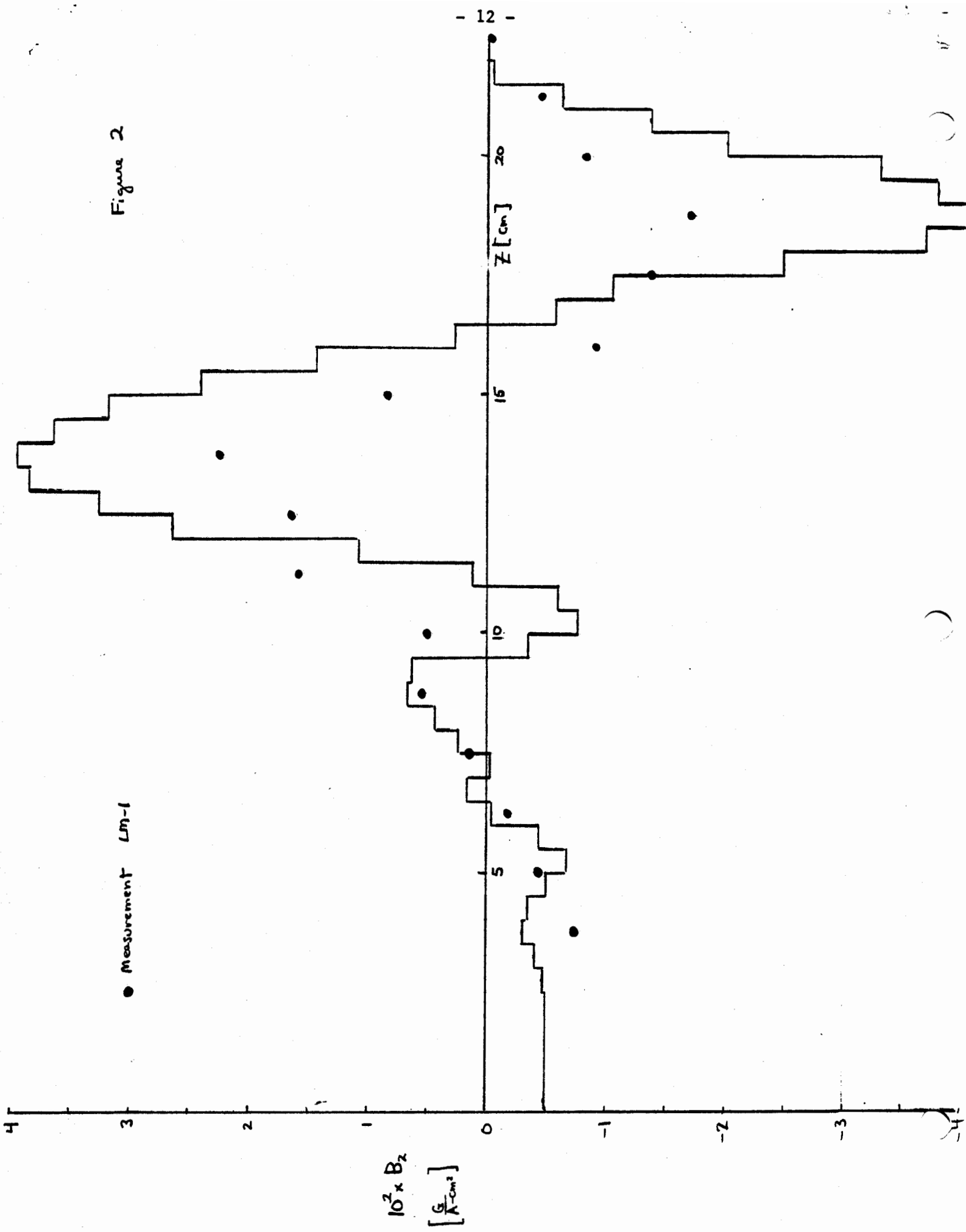
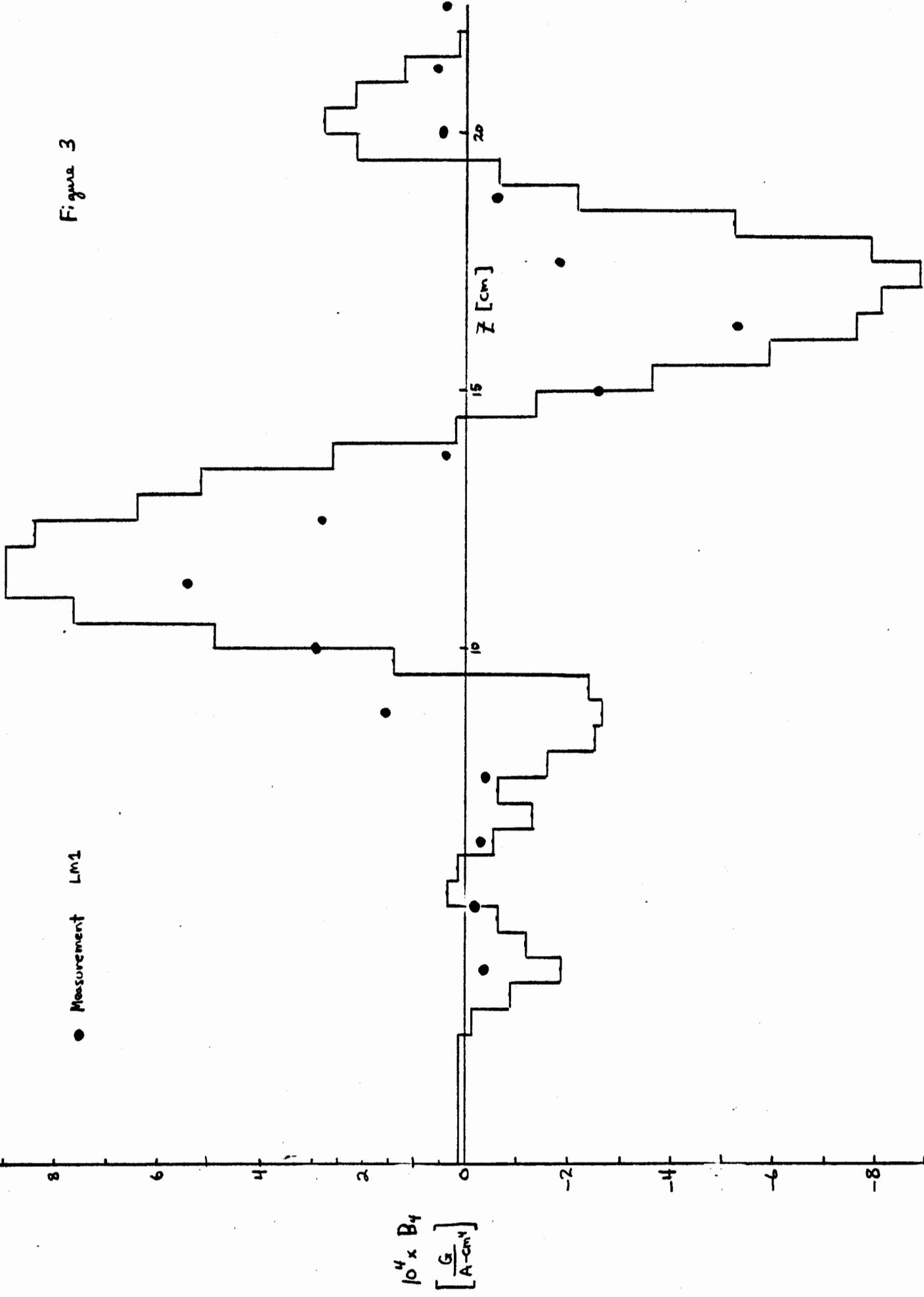


Figure 3

● Measurement LM1



Bldg. 911

H. Fadem
J. Grisoli
H.J. Halama
D. Lazarus
Y. Lee
D. Lowenstein
M. Smith (1) plus
one for each author(s) file
J.R. Sanford
D.H. White

Bldg. 902

M.Q. Barton
H. Foelsche
H. Hahn
R.I. Louttit
R.B. Palmer
E.P. Rohrer
J. Spiro

Bldg. 725

L. Blumberg for
NSLS Library

W.R. Casey, 535A
D.G. Dimmler, 535

Bldg. 510

N. Samios
R.P. Shutt
H. Gordon
T.F. Kycia
L. Leipuner
S. Lindenbaum
S. Ozaki
S. Protopopescu
M. Sakitt
I. Stumer
T.L. Trueman

H. Becker
E. Bleser
R. Engelmann
C. Goodzeit
A. Greene
S. Kahn
J. Kaugerts
H. Kirk
R. Palmer
D. Rahm
R. Shutt
H. Hsieh
M. Tannenbaum
P. Wanderer

/pmb